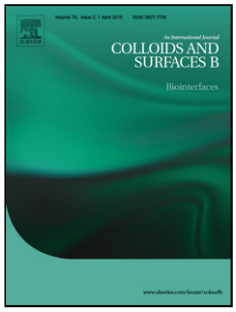

Title: Development of a graphene oxide/chitosan nanocomposite for the removal of picric acid from aqueous solutions: study of sorption parameters

Authors: Mona Mohseni, Hasan Tahermansouri

PII: S0927-7765(17)30668-9
DOI: https://doi.org/10.1016/j.colsurfb.2017.10.019
Reference: COLSUB 8900

To appear in: *Colloids and Surfaces B: Biointerfaces*

Received date: 11-5-2017
Revised date: 5-10-2017
Accepted date: 6-10-2017

Please cite this article as: Mona Mohseni, Hasan Tahermansouri, Development of a graphene oxide/chitosan nanocomposite for the removal of picric acid from aqueous solutions: study of sorption parameters, Colloids and Surfaces B: Biointerfaces https://doi.org/10.1016/j.colsurfb.2017.10.019

Development of a graphene oxide/chitosan nanocomposite for the removal of picric acid from aqueous solutions: study of sorption parameters

Mona Mohseni and Hasan Tahermansouri*

Department of Chemistry, Ayatollah Amoli Branch, Islamic Azad University, Amol, Iran.

Email: h.tahermansuri@iauamol.ac.ir or tahermansuri@yahoo.com

Graphical abstract

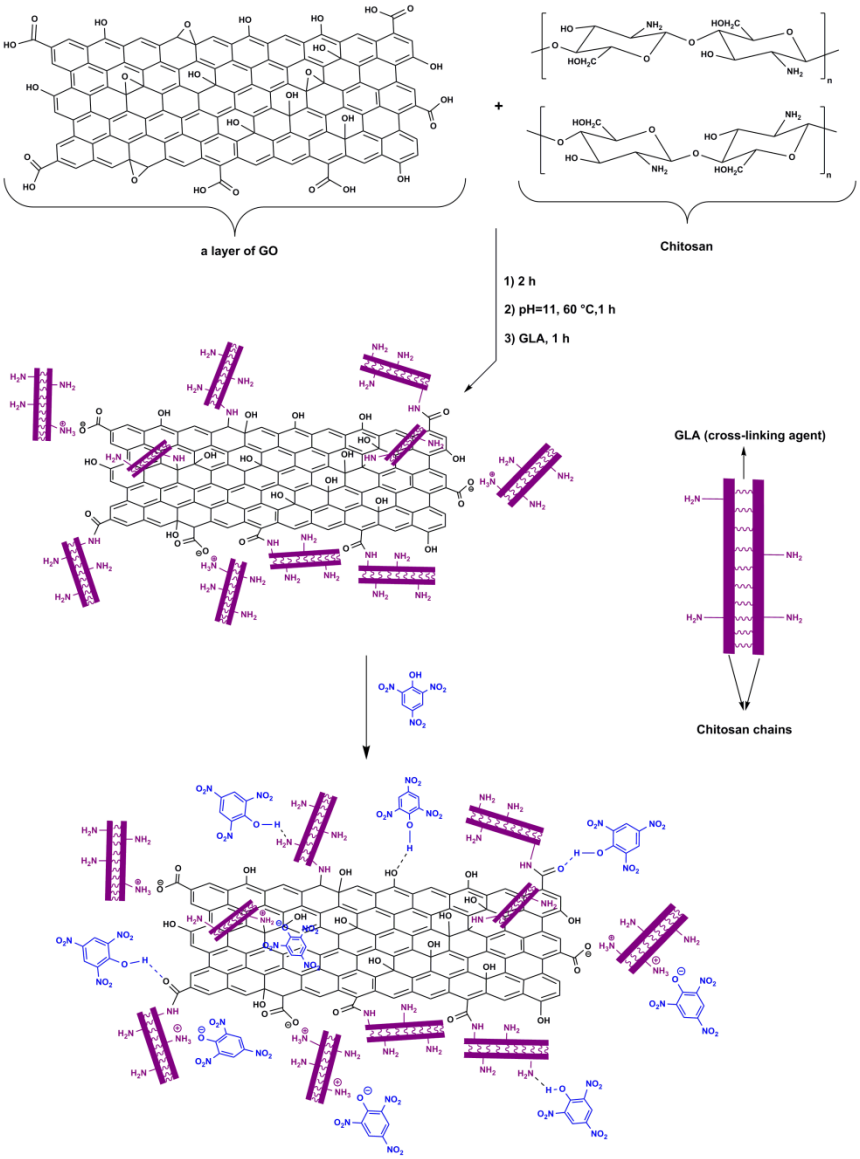

Highlights

- The removal of picric acid using GO-Chi was studied for the first time.
- Sorption process was described by pseudo-second-order kinetic for GO-Chi.
- Freundlich isotherm for GO-Chi was found to best interpretation for sorption data.
- Negative ΔG^o values of GO-Chi indicated the spontaneous nature of sorption process.
- Picric acid molecules can be reused up to 5th cycle of regeneration

Abstract

The functionalization of graphene oxide (GO) with chitosan (Chi) has been investigated to prepare a nanocomposite material (GO-Chi) for the removal of picric acid from aqueous solutions. Materials were characterized by FT-IR, TGA, DTG, FESEM, EDX, XRD and BET. Batch experiments such as solution pH, amount of adsorbents, contact time, concentration of the picric acid and temperature were achieved to study sorption process. Kinetic studies were well described by pseudo-second-order kinetic model for both adsorbents. Isotherm studies showed that the Langmuir isotherm for GO and Freundlich and Halsey models for GO-Chi were found to best represent the measured sorption data. Negative ΔG^o values for GO-Chi and positive ones for GO indicated the nature of spontaneous and unspontaneous, respectively for adsorption process. In addition, picric acid molecules can be desorbed from GO-Chi up to 80% at pH = 9 and that the consumed GO-Chi could be reutilized up to 5th cycle of regeneration.

Keywords: graphene oxide, chitosan, picric acid, adsorption isotherms, thermodynamic, desorption.

1. Introduction

Chitosan (Chi) is a biopolymer in the nature with flexible structure and a great many of functional groups (primary amino and hydroxyl groups) on itself. The presence of amino and hydroxyl groups in the chitosan molecular chain can be used as active adsorption sites in the

removal of various types of contaminants [1,2]. In addition, the review article has been devoted to the removal of heavy metal ions using chitosan [3]. The adsorption performance of chitosan can be improved by its composites. In fact, chitosan composites, which are produced by grafting functional groups of different substances onto the chitosan backbone, such as chitosan-graphene oxide have been advanced to adsorb pollutions from wastewaters [4-14].

Graphene is a kind of laminated material in which only one carbon atom form thickness of single layer of graphite. In the graphitic layers, carbon atoms arrange in a sp^2-bonded network. Graphene oxide (GO) is a graphene-based material with a large number of oxygenated functionalities and high surface area which are the most important features for adsorption processes. Hence, the noteworthy review articles have been dedicated to this topic [15,16].

Phenolic compounds have been found in effluent wastes and rivers since they can be entered by the factories [17]. Thus, they can be effect on the health of humans when are released into the water [18, 19]. Among the phenolic compounds, 2,4,6-trinitrophenol (picric acid) because of its various applications in dyes, explosives, fungicides and military industries, may be entered to water or environment and can be causes a range of health problems since picric acid is toxic even at low concentrations [20-22]. On the other hand, the World Health Organization (WHO) and USEPA reported 0.001 mg/L as the permissible phenolic concentration in potable water and 0.1 mg/L permissible limit in wastewater, respectively [23,24]. Therefore, removal of picric acid from aqueous solutions became a major focus of research and is essential.

In the recent years, many studies have been carried out to removal of nitrophenolic compounds from aqueous solutions by different adsorbents which can be cited olive wood [25], organoclays [26,27], nano zeolite [28,29], biochar [30], carbon nanotubes [31], nano graphite oxide [32], date seeds [33] and actived carbon [34]. However, only a few reports have been presented on the removal of picric acid from aqueous solutions [35-39]. Also, Table 1 shows some adsorbents for the removal of nitrophenolic compounds under different experimental conditions. Taking this background into account and considering the toxic activities of picric acid for humans, the purpose of the present work was to study the removal of picric acid from aqueous solutions by graphene oxide-chitosan (GO-Chi) nanocomposite. In this current study, GO-Chi nanocomposite, consisted of cross-linked chitosan and GO, was prepared and characterized with various techniques such as Fourier transform infrared spectroscopy (FT-IR), thermogravimetric analysis (TGA), derivative thermogravimetric

(DTG), field emission scanning electron microscopy (FESEM), energy dispersive X-ray analysis (EDX), X-ray diffraction (XRD) and Brunauer-Emmett-Teller (BET) surface area analyzer. Then, GO-Chi was applied as an efficient adsorbent for the removal of the picric

Adsorbents	Type of pollutions	Efficiency of adsorbent	Ref
Montmorillonites modified with hexamethylene bispyridinium dibromides	phenol, *p*-chlorophenol, *p*-methylphenol, *p*-nitrophenol	the uptake of phenols decreased in the order: phenol > *p*-chlorophenol > *p*-methylphenol > *p*-nitrophenol	[27]
Fe-nano zeolite	*m*-, *o*- and *p*-nitrophenol	Adsorption capacity of *m*-, *o*- and *p*-nitrophenol were 168.7, 193.9 and 223.1 mg/g, respectively	[28]
nano zeolite	*m*-, *o*- and *p*-nitrophenol	The adsorption capacities of nitrophenols ranged from 121.7 to 156.6 mg/g.	[29]
Fe/Zn-biochar	*p*-nitrophenol	The results showed that Fe/Zn-biochar has larger PNP adsorption capacity under acidic pH solution	[30]
nanographite oxide	p-nitrophenol	The maximum adsorption capacity was 268.5 mg/g at 283 K and a natural pH	[32]
date seeds	2,4-Dinitrophenol	The regeneration efficiency of date seeds was 96% compared to 85% of activated carbon	[33]
activated carbon	phenol and 2,4-dinitrophenol	The adsorption capacity value for phenol and 2,4-dinitrophenol were 1.628 and 3.614, respectively.	[34]
Amberlite IRA-67	Picric acid	The removal of acid was estimated about 65-67%	[35]
silicate MCM-41	Picric acid	The adsorption capacity of picric acid varied significantly with the pH of the solution	[36]
magnetic activated carbon	Picric acid	The adsorption capacity of picric acid was estimated about 65-74 mg/g	[37]
hydrotalcite	Picric acid	The adsorption maximum was estimated 750-2250 μmol/g	[39]
MWCNT-COOH	Picric acid	The adsorption capacity of picric was calculated about 27.7 mg/g	[31]

Table 1. Literature results of the nitrophenolic adsorption by different adsorbents.

acid from aqueous solutions. In this research, the four models of kinetic, pseudo-first order, pseudo-second-order, Elovich and intra-particle diffusion models and four adsorption isotherm models (Langmuir, Freundlich, Halsey, Tempkin,) were studied to get an adequate understanding on the mechanism and rate of the adsorption process of picric acid on the GO-

Chi. In fact, the goal of this investigation was to compare GO and GO-Chi nanocomposite as adsorbent for removal of picric acid from aqueous solutions.

2. Experimental

2.1. Materials and methods

Chitosan with low molecular weight ($M_W = 1.08 \times 10^5$, degree of deacetylation = 81%) from Sigma-Aldrich, Picric acid, ammonia and glutaraldehyde (GLA) from Merck Chemical Inc. and graphene oxide nanoplatelets (99%, Thickness 3.4-7 nm with 6-10 Layers) were purchased and used as received. Analytical reagent-grade chemicals were used as well as deionized water from a Milli-Q system (Millipore). The concentration of picric acid was determined by Unico UV-2100 Model variable-wavelength UV-Vis spectrophotometric at 340 nm. Field emission scanning electron microscope and energy dispersive X-ray analysis measurements were taken using an MIRA3\\TESCAN-XMU model. Fourier transform infrared spectroscopy was recorded using KBr tablets on a Thermo Nicolet Nexus 870 FTIR spectrometer. The samples were studied by thermogravimetric analysis (Netzsch TG 209 F1 Iris1) under nitrogen gas atmosphere (10˚C/min). X-ray diffraction measurements were acquired on a Bruker D8 advance diffractometer using Cu-Ka radiation (λ =0.154 nm). The nitrogen adsorption-desorption experiments were carried out at 77 K by using BELSORP Mini II instrument, and the surface area was calculated by the Brunauer-Emmett-Teller (BET) method with a 16-point BET plot of a nitrogen adsorption at 77 K, and the pore distribution was measured by the Barrett-Joyner-Halenda (BJH) model.

2.2. Synthesis of GO-Chi nanocomposite

For the preparation of the GO-Chi nanocomposite, 0.5 g of GO with 200 mL of chitosan solution (0.5 g of Chi dissolved in 500 mL of 2 % (v/v) acetic acid solution) was mixed. The obtained suspension was sonicated for 30 min and thus the mixture was stirred vigorously for 2 h until the homogenous solution was obtained. Afterward, the pH of the reaction mixture was adjusted to 10-11 with addition of ammonia (1% v/v) to precipitate the chitosan and was heated to 60 °C for further 1h. Then, 1 mL of GLA was added into the reaction mixture for the cross-linking of Chi and the mixed system was stirred continuously for other 1h. Black

products was collected by centrifugation and washed with diluted acetic acid and distilled water to remove uncross-linked Chi. In finally, the black powder of the obtained GO-Chi was dried at 60 °C overnight.

2.3. Batch sorption experiments

To study the effects of pH on the sorption of picric acid, 30 mg of GO or GO-Chi was dispersed into 15 mL solutions containing 100 mg/L of picric acid. The initial pH values were adjusted from 3.0 to 9.0 using nitric acid and NaOH at 25±1 ˚C. The amounts of sorbed picric acid were calculated as the difference between the initial and final concentrations when the equilibrium was reached. The results are based on at least three replicate experiments for each pH value. To estimate the sorption capacity, 20 mg of GO or GO-Chi was mixed with 15 mL of picric acid solution (concentration range 10-100 mg/L). After 5h, the picric acid concentration in the aqueous solutions was determined by UV-Vis spectroscopy. The removal (%) and sorption capacity q (mg/g) was obtained as follows:

$$\text{Removal } \% = \frac{C_0 - C_e}{C_0} \times 100\% \qquad q_e = \frac{(C_0 - C_e) \times V}{m}$$

where C_0 and C_e are the initial and final concentrations (mg/L) of picric acid in the aqueous solution, respectively, V (L) is the volume of picric acid solution, and m (g) is the weight of sorbent. The kinetic experiments were carried out under normal atmospheric conditions at 25±1˚C. Initially, 30 mg of GO or GO-Chi was contacted with 15 mL solution containing 100 mg L^{-1} picric acid concentration in glass vials and then it were stirred for the different times. Adsorbent and solution were separated at predetermined time intervals and analyzed for residual picric acid concentrations as described in above. The thermodynamic experiments were carried out at different temperatures (25, 40 and 50 ºC) and the used values were similar to kinetic ones.

2.4. Kinetic models

Kinetic models such as pseudo-first-order, pseudo-second-order, Weber-Morris intra-particle diffusion and Elovich models were employed to investigate the rate of the adsorption process and rate-controlling step. The best-fit model is selected based on the correlation coefficient values (R^2) of the linear regression.

2.4.1. pseudo-first-order model

The pseudo-first-order equation has been used for low concentration of solute [40] and it was proposed by Lagergren [41]. The linear form of this equation is expressed as follows:

$$\log (q_e - q_t) = log\ (q_e) - \frac{K_1}{2.303}\ t \qquad (1)$$

where k_1 is the rate constant of adsorption (min^{-1}), q_e is the amount adsorbed (mg/g) at equilibrium and q_t is the amount adsorbed (mg/g) at time t. The plot of log (q_e - q_t) against t gives a linear relationship from which k_1 and q_e are determined from the slope and intercept of plot, respectively.

2.4.2. pseudo-second-order model

The pseudo-second-order model in linear form may be expressed as given [42,43]:

$$\frac{t}{q_t} = \frac{1}{k_2 q_e^2} + \frac{1}{q_e}\ t \qquad (2)$$

where k_2 is the pseudo second-order rate constant of adsorption (g/mg min), other terms has already been defined. The values of q_e and k_2 can be estimated from the slope and intercept of the plot of t/q_t versus t.

2.4.3. Elovich's model

Elovich's equation [42,44] describes chemisorption processes and usually applied to the heterogeneous surfaces of adsorbent which energetically are different and that at low surface coverage, the desorption and interaction don't occur between the adsorbed species. This model can be expressed to the linear form as follows:

$$q_t = \frac{1}{b}\ln(ab) + \frac{1}{b}\ln(t) \qquad (3)$$

The parameter a of the equation is the initial sorption rate (mg g^{-1} min^{-1}), while the parameter b is related to the extent of surface coverage and activation energy for chemisorption (g mg^{-1}). If this equation applies, it should lead to a straight line which a and b coefficients can be calculated from the plot of q_t versus ln t.

2.4.4. Intra-particle diffusion model

In order to the precise investigation and better understanding of the adsorption mechanism that affect the kinetics of adsorption, the kinetic data were fitted to Weber-Morris intra-

particle diffusion model [43, 45]. Indeed, it is described by external mass transfer and intra-particle diffusion. This model is expressed as follows:

$$q_t = k_{id} t^{0.5} + C_i \qquad (4)$$

where k_{id} (mole $g^{-1}min^{1/2}$) is the rate constant of intra-particle diffusion and C_i is proportional to the boundary layer thickness. If the regression of q_t versus $t^{1/2}$ gives a straight line, then intra-particle diffusion is involved in the adsorption process and if this line passes through the origin, then intraparticle diffusion is the sole rate-limiting step and k_{id} can be calculated from the slope and C_i from the intercept.

2.5. Isotherm models

2.5.1. Langmuir isotherm

The Langmuir model [43, 46] assumes which the maximum sorption capacity corresponds to complete monolayer coverage of the molecules on the adsorbent surface, with no interaction between sorbed molecules. In addition, this empirical model refers to the same activation energy of adsorption when the adsorption of each molecule occurs at definite localized sites onto a homogeneous surface without transmigration of adsorbate in the plane of the surface. Langmuir equation in non-linearized form can be written as follows:

$$q_e = \frac{b q_m C_e}{1 + b C_e} \qquad (5)$$

where q_e (mg g^{-1}) and C_e (mg L^{-1}) are the amount of solute adsorbed per unit weight of adsorbent at equilibrium and picric acid concentration at equilibrium, respectively. q_m (mg g^{-1}) is the maximum adsorption capacity, and b is the adsorption equilibrium constant (L mg^{-1}) that is related to the free energy of adsorption. The linearized form of the Langmuir equation is:

$$\frac{C_e}{q_e} = \frac{1}{b q_m} + \frac{C_e}{q_m} \qquad (6)$$

Also, the dimensionless equilibrium parameter or separation factor, R_L, is the essential characteristics of Langmuir isotherm as follows [42]:

$$R_L = \frac{1}{1 + b C_0} \qquad (7)$$

where b is the Langmuir constant and C_0 is the initial concentration of adsorbate in solution.

2.5.2. Freundlich and Halsey isotherms

Freundlich [47] and Halsey [48] isotherms can be used to multilayer adsorption and the heterogeneous surfaces with non-uniform distribution of adsorption heat [49]. The linearized form of the Freundlich equation is:

$$ln\, q_e = lnK_f + \frac{1}{n} lnC_e \qquad (8)$$

where K_F is an empirical constant related to the sorption capacity of the adsorbent (L mg^{-1}) (L g^{-1})$^{1/n}$ and constant n is a constant indicative of the intensity of the adsorption and varies with surface heterogeneity and affinity. Also, n values between 1 and 10 and less than 1 represent favorable and poor, respectively, sorption process. The values of k_f and n can be calculated by plotting ln q_e versus ln C_e. Also, Halsey equation can be given as:

$$ln\, q_e = \frac{1}{n_H} ln\, K_H - \frac{1}{n_H} ln \frac{1}{C_e} \qquad (9)$$

where K_H and n_H are the Halsey constants, which can be obtained from the slope and the intercept of the linear plot based on ln(q_e) versus ln $1/C_e$, respectively.

2.5.3. Tempkin isotherm.

Tempkin et al. [50] suggested that due to adsorbent-adsorbate interactions, the heat of adsorption of all molecules linearly decrease with the surface coverage and that the adsorption is characterized by a uniform distribution of the binding energies, up to some maximum binding energy. The linearized form of Tempkin model was generally applied in the following formula:

$$q_e = K_1\, ln\, K_2 + K_1\, ln\, C_e \qquad (10)$$

where k_1 is related to the heat of adsorption (L/g) and K_2 is the dimensionless Tempkin isotherm constant. Tempkin parameters (k_1 and k_2) can be determined from the linear plots of q_e versus ln C_e.

2.6. Desorption and reuse of GO-Chi

The adsorption was done in 15 mL of 100 mg L^{-1} picric acid solution with 30 mg of GO-Chi at 25 ˚C for 5 h. After filtration, the desorption carried out at a pH range of 3 to 9. On the basis, the GO-Chi was immersed in 15 mL of 1 mol L^{-1} NaOH or HNO_3 aqueous solution and agitated at 25 ˚C for 5 h. Then, the GO-Chi was removed from the solution and washed with water for reutilization. Thus, released picric acid values in the aqueous solutions were determined by UV-Vis spectroscopy.

3. Results and discussion

3.1. Characterization of the adsorbents

The adsorbents were characterized using FT-IR, TGA, DTG, FESEM, EDX, XRD and BET. The chemical structures of GO and GO-Chi were determined by FT-IR analysis as presented in Fig. 1a. In GO, the peaks at 1700-1735 and 1621 cm^{-1} are assigned to the C=O stretching vibration and C=C stretching mode of the sp^2 carbon skeletal network or epoxy groups, respectively. In addition, the absorption peaks at 3439 and 1042-1168 cm^{-1} clearly are stretching vibration of hydroxyl groups and the C-O vibration of various oxygen-containing groups such as epoxy and carboxyl group, respectively. These results show that plenty of hydroxyl, carboxyl, and epoxy groups were located on the graphene oxide. In the spectrum of GO-Chi, the carboxyl peak at 1735 cm^{-1} disappeared and the remarkable peaks at around 1628, 1570 and 1403 cm^{-1} appears which can be assigned to C=O stretching vibrations of -NHCO, N-H bending vibration of amino and stretching vibration of carboxylate groups ($^{-}$O-C=O). In addition, the intensity of later absorbance bands is significant which can be related to the reaction of the oxygen-contained functional groups of GO with amino groups of Chi which follow the increase of the intensity of absorption peaks. These alterations could be related to the reaction of GO carboxyl groups with amino groups of Chi in order to form amides (band at 1628 cm^{-1}) and carboxylate groups (band at ~1403 cm^{-1}), and that of Chi amino groups with GO epoxy groups which result in the formation of amino groups (NH, peak at 1570 cm^{-1}). In addition, we confirmed the formation of covalent bonds between GO and Chi by comparing the IR spectrum of GO-Chi with that of GO/Chi mixtures. As can be seen, there is not the remarkable peak at 1570 cm^{-1} in GO/Chi as compared to GO-Chi spectrum. Also, the carbonyl peak at 1738 cm^{-1}, which there is in GO/Chi spectrum, was disappeared in GO-Chi spectrum. This results demonstrate the covalent interactions between GO and Chi. Therefore, the functionalization of GO with Chi by FT-IR spectra was successfully confirmed.

TGA is a valuable tool to characterize the modified GO which present quantitative and useful information concerning the modification of GO. As shown in Fig. 1b (a), TGA curve of GO display 8.86% of mass loss below 120 °C which can be assigned to the evaporation of adsorbed water on the graphene oxide. In addition, one rapid mass loss occurred at around 130-210 °C with a weight loss about 11.51% that arise from the removal of the oxygen-containing functional groups. Also, it shows a gradual trend in decomposition from 210 to

650 ˚C with a weight loss of about 32.5 % that can be assigned to the further removal of functional groups (probably carboxylic groups). In TGA of GO-Chi, one major decomposition at around 160-650 °C with a weight loss about 32.69% is observable which can be assigned to decomposition of the cross-linked chitosan. On the basis, the mass ratio between chitosan and GO was estimated 1(chitosan) to 1.82 (GO).

DTG curve of provides further evidence for modification. In Fig. 1b (b), the major peaks at

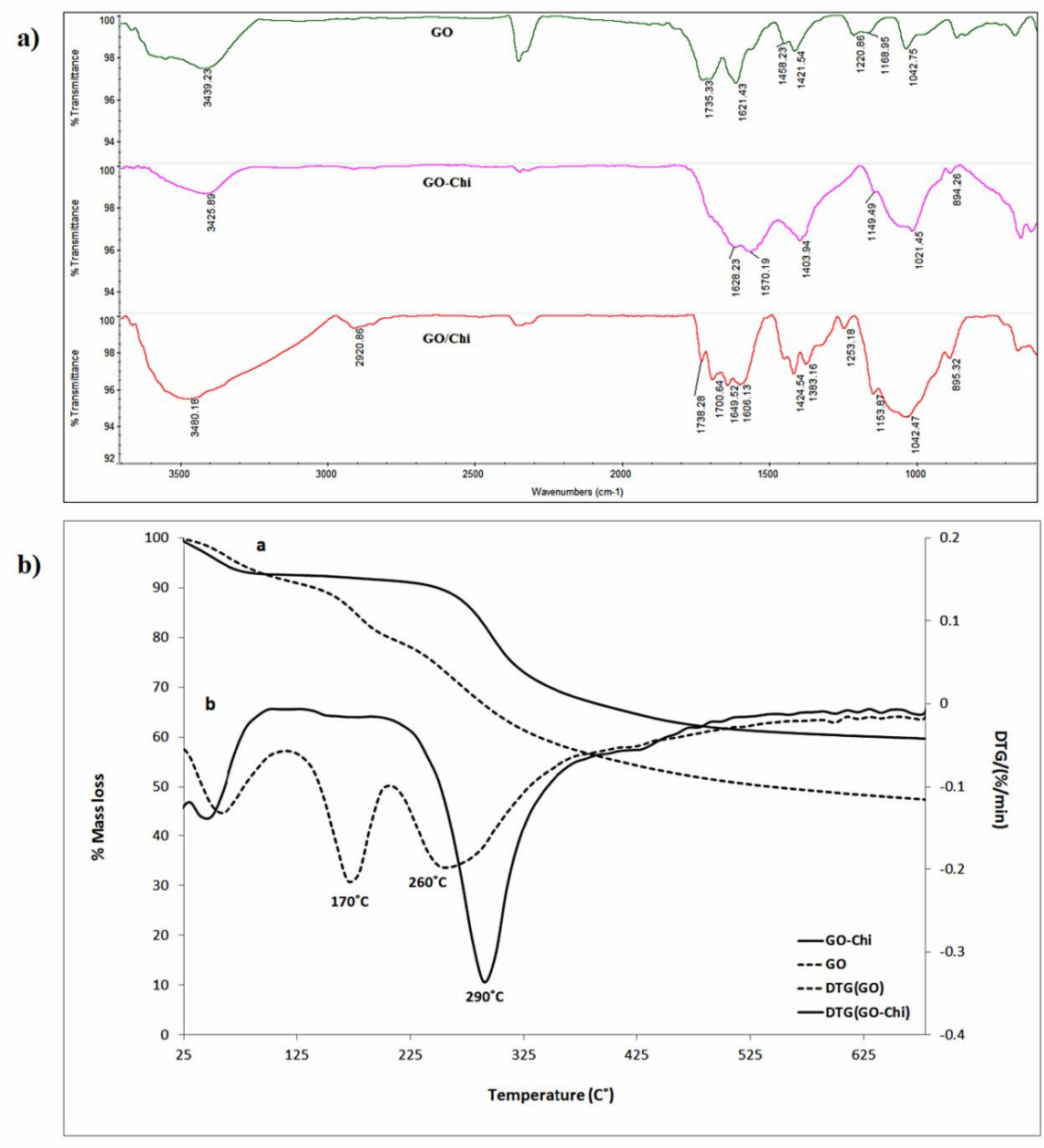

Fig. 1. (a) FT-IR spectra (after baseline correction) of GO, GO-Chi and GO/Chi. (b)TGA (a) and DTG (b) curves of GO and GO-Chi in the N_2 (10˚C/min).

170 and 260˚C for GO could be attributed to the decomposition of the oxygen and carboxyl groups, respectively bonded to GO. On the other hand, the peak at 290 ˚C for DTG curve of GO-Chi can be assigned to the cross-linked chitosan decomposition. These results indicate which Chi has been situated onto the GO nanosheets.

FESEM images of GO and GO-Chi were presented in Fig. 2a. It can be found clearly that GO sheets present the sheet-like structure with large thickness, smooth surface, and wrinkled edge. After the combination with Chi to form the GO-Chi nanocomposite, a rougher surface is existed. Also, it shows that Chi was inserted between the graphene layers which confirm the functionalization of the GO layers with Chi. In addition, the elemental analysis of GO and GO-Chi evaluated by EDX. As can be seen in Fig. 2b, GO contains carbon, oxygen, sulfur, chlorine and a little value of nitrogen. Three later elements are the consequence of sulfuric acid, hydrochloric acid, sodium nitrite or other materials which are probably used for GO synthesis. Higher carbon content was determined in GO (48 wt.%) versus GO-Chi (43 wt.%). On the other hand, high nitrogen content was estimated in GO-Chi (11.88 wt.%) versus GO (2.66 wt.%). In addition, the elemental percentage of oxygen was 43.55% and 43.43% for GO and GO-Chi, respectively. Also, the atomic percentages are presented into the EDX curves for the comparison. This finding approximately is consistent with the reported percentages in the literatures [5, 10]. These results confirmed the modification of GO with Chi.

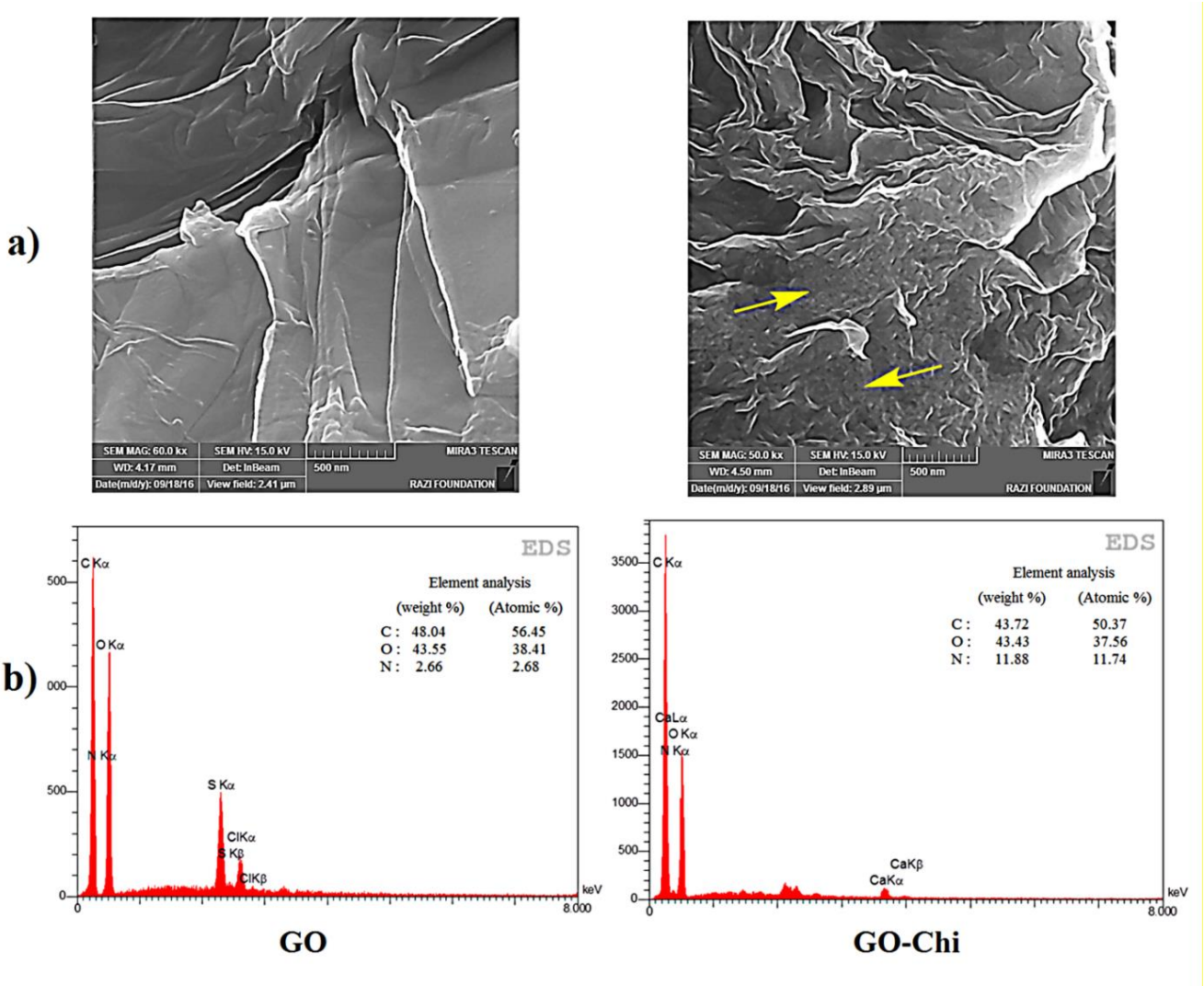

Fig. 2. (a) FESEM and (b) EDX images of the GO and GO-Chi. The yellow arrows show the inserted chitosan molecules between graphene layers.

The X-ray diffraction (XRD) spectra of GO and GO-Chi are given in Supplementary materials. The characteristic XRD peak of GO is observed at $2\theta = 11.17^{\circ}$ which corresponds to a d-spacing of 0.791 nm as estimated by Bragg's law [51, 52]. It can be related to the large amount of polar functional groups generated between graphene layers during oxidation. In addition, the pattern of the GO-Chi displayed a broad peak at $2\theta = 20.27^{\circ}$, attributed to the amorphous-like structure of Chi and the characteristic peak of GO at $2\theta = 10.26^{\circ}$, demonstrating the presence of two phases in this nanocomposite [53]. Thus, these results indicate that Chi biopolymer was successfully introduced between the GO layers.

The results of Nitrogen adsorption-desorption isotherm at 77 K for the GO and GO-Chi along with the porous structure parameters are shown in Fig. 3. On the basis of IUPAC classification [54], the pores of porous materials can be divided into micropore (size less than

2 nm), mesopore (size between 2 and 50 nm) and macropore (size greater than 50 nm). As can be seen from Fig. 3, the adsorbed nitrogen volume by GO-Chi was larger than that by GO, indicating a higher porosity for GO-Chi. On the other hand, according to the original IUPAC classification [54], the curves of both adsorbents are classified as type IV isotherms which confirmed the presence of mesoporous structure. In addition, the hysteresis loop of GO and GO-Chi exhibited the H3 and H1 type curves, respectively. It shows which the pore shapes of GO and GO-Chi are narrow slit-shaped and cylinder-shaped mesopores, respectively. The BET surface areas of GO and GO-Chi are presented in Fig. 3. As shown in Fig .3, BET surface areas of the graphene increased when Chi was added. In other words, the surface area increases from 155.27 to 376.1 m^2g^{-1} after inserting Chi into graphene sheets. In addition, total pore volume and pore size for GO 0.4586 cm^3g^{-1} and 2.42 nm, and those for

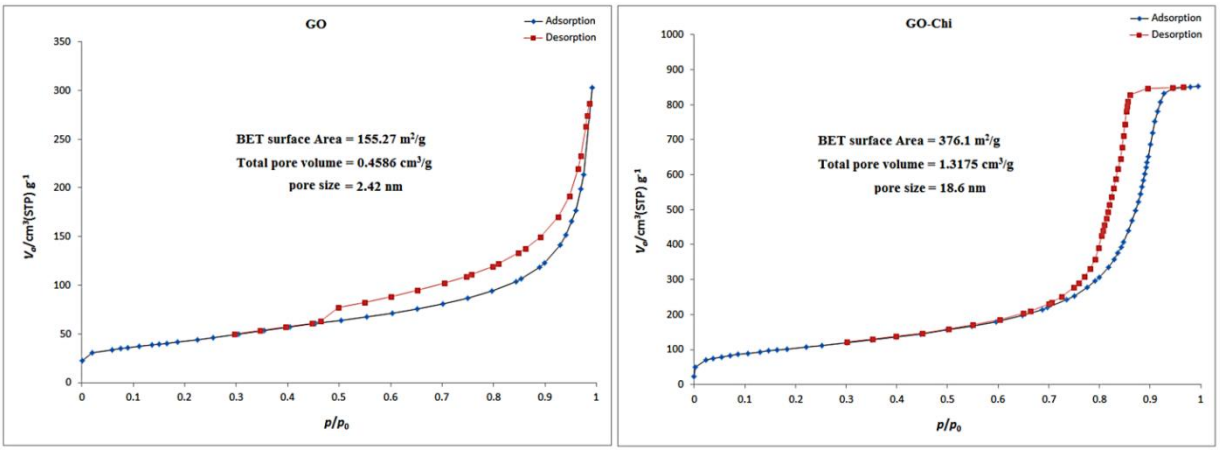

Fig. 3. Typical N_2 adsorption/desorption isotherm and pore structure parameters of GO and GO-Chi.

GO-Chi 1.3175 cm^3g^{-1} and 18.6 nm, respectively was obtained. Moreover, it was remarkable that when Chi was introduced on the GO, pore volume and size increased. These results can be related to insertion of Chi particles onto the surface of graphene sheets, which enlarge the distance between layers of graphene sheets. Hence, surface area of the nanocomposite increased. It topic causes the increase of adsorption capacity of the picric acid by GO-Chi which is discussed later in this article.

3.2. Adsorption studies

3.2.1. Sorption kinetic

The removal percentage of picric acid by GO and GO-Chi was studied as a function of contact time, as shown in Fig. 4a. At up to 20 min for the GO and 30 min for the GO-Chi of

initial contact time, the adsorption rate of picric acid on the both adsorbents was relatively rapid and then reached equilibrium at nearly 60 min for GO and at 180 min for GO-Chi. The fast initial removal indicates a high interaction of treated sorbent with picric acid. The final value of the removal percentage of picric acid for the GO and GO-Chi was found to be 21.2% and 71.6%, respectively. These values indicate which adsorption capacity of picric acid for the GO-Chi is more than that of GO. The fast adsorption in the initial stage can be related to the presence of a large number of vacant adsorption sites in which picric acid molecules can easily interacted with these sites. After a period of time, the remaining vacant sites are difficult for the picric acid molecules to occupy which this phenomenon can be related to the repulsion between the adsorbed picric acid molecules on the graphene and bulk phases, which it causes a long time to reach equilibrium, in particular for GO-Chi.

Table 2 shows the calculated values of the adsorption parameters for the pseudo-first-order equation (K_1 and q_e), the pseudo-second-order equation (K_2, q_e) and Elovich's equation (a and b). In addition, all plots of adsorption kinetics were presented in Supplementary data. As can be seen from Table 2, the pseudo-first-order and Elovich models have the low correlation coefficients, R^2 for both adsorbents. It shows unsuccessful of these models to fit the experimental data. The correlation coefficients of the pseudo-second-order model for GO and GO-Chi are calculated 0.9994 and 0.9948, respectively which indicate the suitability of the pseudo-second-order equation for sorption of picric acid by both adsorbents. In addition, the sorption capacity of picric acid at equilibrium (q_e) for GO and GO-Chi were 10.87 and 39.52 mg g^{-1}, respectively which agree well with the corresponded experimental data (10.6 mg g^{-1} for GO and 35.8 mg g^{-1} for GO-Chi). These results show that the sorption of picric acid from an aqueous solution onto GO and GO-Chi obeys the pseudo-second-order kinetic model and could be used to determine the equilibrium sorption capacity, rate constants, and the percentage of picric acid removal.

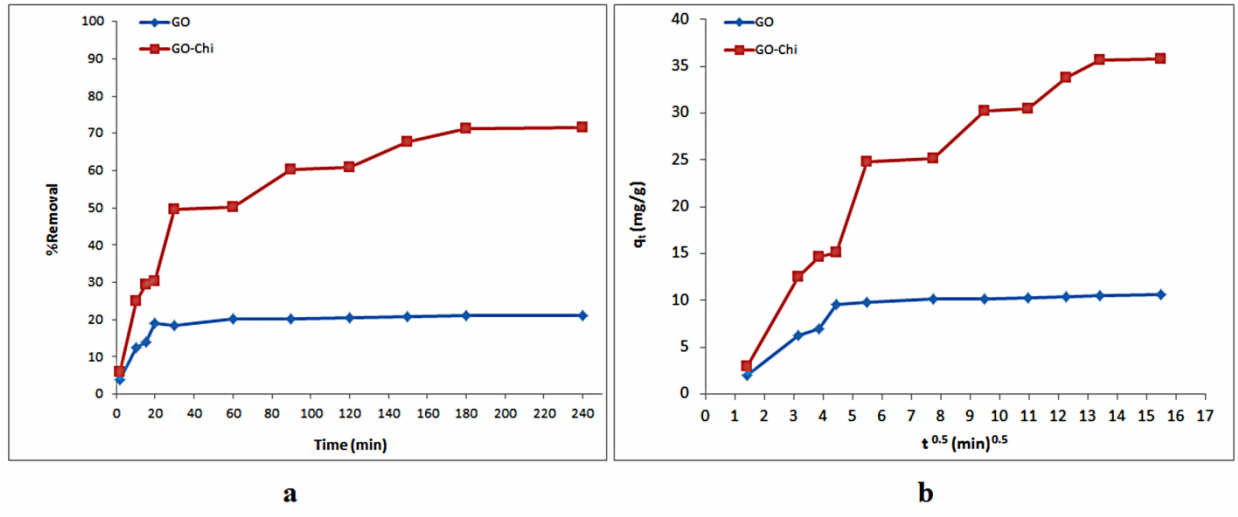

Fig. 4. (a) Effect of contact time on the removal of picric acid from aqueous solution by both adsorbents (experimental conditions: pH=7; adsorbent mass, 30mg/15 mL; picric acid concentration, 100 mg/L). (b) Linearized intra-particle diffusion kinetic model of picric acid sorption onto GO and GO-Chi**.**

Fig. 4b indicates the plots of the intra-particle kinetic model of picric acid sorption by GO and GO-Chi. According to Fig 4b, the plots of both adsorbents have the nonzero intercepts which show intra-particle diffusion is not the rate-limiting step of the sorption process. Hence, this model is not the only rate-controlling step. The deviation of the straight lines from the origin can be related to the difference in the rate of mass transfer during the initial and final stages of adsorption. In addition, the plots contain two different lines which present the mechanism of two stages for intra-particle diffusion of picric acid within GO and GO-Chi. The initial adsorption stage starts from 0 to 4.5 (20 min) for GO and 0 to 5.5 (30 min) for GO-Chi which is approximately rapid for both adsorbents. On the other hand, the second stage is milder and more gradual and is from 4.5 to 7.7 (20 to 60 min) for GO and from 5.5 to 13.4 (30 to 180 min) for GO-Chi. These phenomena could be attributed to the fast diffusion of the picric acid from the aqueous phase to the outer-surface of adsorbents for first stage and the intra-particle diffusion of the picric acid molecules into the porous structure of the graphene for the second stage. In other words, when the adsorption of exterior surface reached to saturation, picric

Table 2. Parameters of pseudo-first-order, pseudo-second-order, Elovich and intra-particle diffusion models for picric acid sorption onto both adsorbents. Temperature, 298 K; initial picric acid concentration, 100 mg L^{-1}; mass of adsorbents, 30 mg; volume of solution, 15 mL; and pH of the sample solution, 7.0.

	Pseudo-first-order model			**Pseudo-second-order model**			**Intra-particle diffusion model**		**Elovich model**			
Adsorbents	**k_1(min^{-1})**	**q_e(mg/g)**	**R^2**	**K_2(g $mg^{-1}min^{-1}$)**	**q_e(mg/g)**	**R^2**	**K_{id}(mg g^{-1} $min^{-0.5}$)**	**R^2**	***a***	***b***	**R^2**	**$q_{e,ex}$**
GO	0.0205	3.40	0.8319	0.0147	10.87	0.9994	0.4392	0.5801	7.54	0.5989	0.8355	10.6
GO-Chi	0.0223	33.45	0.8781	0.0010	39.52	0.9948	2.2234	0.9010	4.43	0.1367	0.9721	35.8

acid molecules entered into the pores of the adsorbent and were adsorbed by the interior surface of the mesopores. Overall, these results confirmed which the intra-particle diffusion model is not the only rate-controlling step and that both the external surface sorption and intra-particle diffusion participate in the process of the picric acid adsorption. The results are shown in Table 2.

3.2.2. Effect of adsorbent dosage

In order to determine the adsorption percentage of picric acid from aqueous solutions at a picric acid concentration of 100 mg/L, we studied dosage effect. According to Fig. 5a, the adsorption percentage of picric acid by GO-Chi enhance with increasing its dosage so that the removal of picric acid significantly increased from 34.6% to 90.6% when the dosage of GO-Chi increased from 0.01 g to 0.07 g. However, these values for GO are not remarkable since increasing the GO dosage cause a little increment in sorption of picric acid (13.5% to 22.4%). This increase for GO-Chi can be correlated to the presence of a large number of accessible sites in GO-Chi in the high dosage as compared to GO.

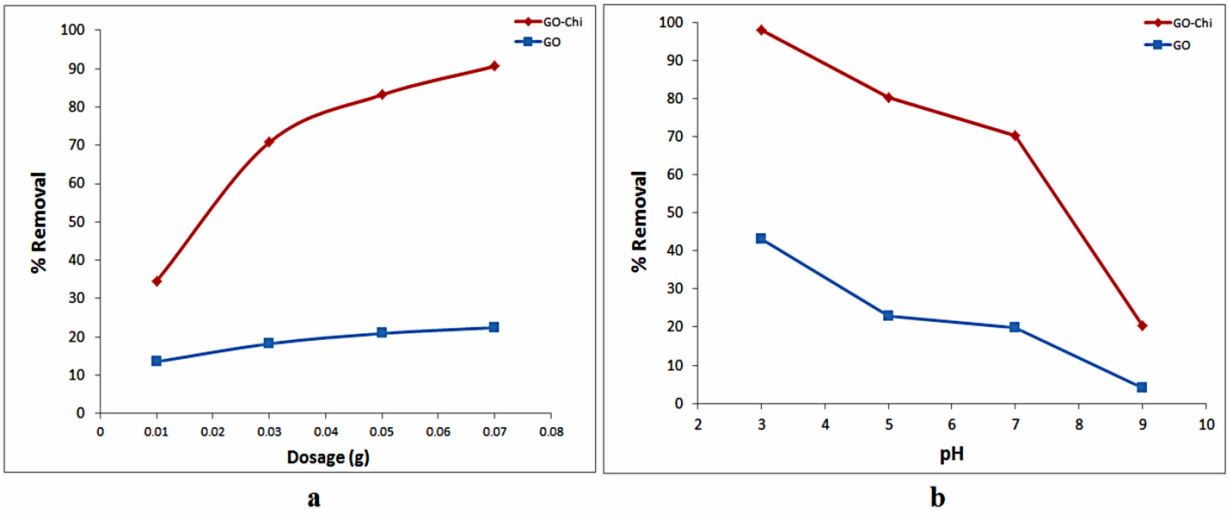

Fig. 5. (a) Effect of adsorbent dosage on the adsorption of picric acid from aqueous solution (experimental conditions: pH 7; contact time, 5 h; picric acid concentration, 100 mg/L, volume, 15 mL). (b) Effect of initial pH on picric acid sorption onto GO and GO-Chi.

3.2.3. Effect of pH

Effect of pH on the uptake of picric acid is shown in Fig. 5b. Since adsorption studies in drinking water purification were more significant in the neutral pH, we in this study have calculated the adsorbed values of picric acid after equilibrium at C_0=100 mg/L in the range

between 3 and 9 for the comparison purpose. In liquid-phase adsorption, the adsorption capacity of GO and GO-Chi for aromatic compounds depends on a number of factors such as the physical nature of the adsorbent (pore structure, purity and functional groups), the nature of the adsorbate (its solubility, the presence of functional groups, polarity, molecular weight and size) and the solution conditions such as pH. The experimental results of adsorption in the various pH suggested that there is an increase in the uptake of picric acid in pH = 3. It can be related to the solubility of picric acid in the aqueous solutions which is dependent on the pH values. In fact, the solubility of picric acid diminishes with the decrease of pH value or the increase of concentration H^+ since the adsorption of phenolic compounds on the activated carbon has inversely proportional to solubility [31]. Therefore, the adsorption percentage of picric acid by the GO and GO-Chi increased with the decrease of pH value. On the other hand, the picric acid (pK_a= 0.4) dissociates to picrate anion in the higher pH values in which the surface functional groups are either neutral or negatively charged (pK_a = 6.5 for Chi). In these conditions, the electrostatic repulsion between the identical charges decreases the adsorption capacity. In addition, since the picrate anions are more soluble in the aqueous solution, the stronger adsorbate-water bonds must be broken before adsorption can be occurred [55]. Therefore, the adsorption of picric acid decreases in the higher pH.

3.3. Adsorption isotherms

The ratio between the adsorbate concentrations in the solid and liquid phases at a constant temperature was introduced as adsorption isotherms which are explained as the mathematical equations. In fact, it indicates how a substance from the aqueous media transfers to a solid phase when an equilibrium state is established in system. In this study, the isotherm models of Langmuir, Freundlich, Halsey and Tempkin along with their constant values, which describe the surface properties and affinity of the adsorbent, have been used to express the mechanism of adsorption. All plots of adsorption isotherms are presented in Supplementary data.

The linear form of the Langmuir model with its parameters is shown in Table 3. The values of the obtained regression coefficients for both adsorbents indicate which the Langmuir model well describes adsorption of picric acid onto GO but that is not suitable for GO-Chi since its regression coefficient is low. In other words, only GO because of high regression coefficient confirms which the adsorption is a monolayer process and it requires equal activation energy for all species. In addition, the calculated values of R_L for both adsorbents

are shown in Supplementary data. These values show the type of isotherm to be irreversible ($R_L = 0$), favorable ($0 < R_L < 1$), linear ($R_L = 1$) or unfavorable ($R_L > 1$). The R_L values were found to be at around 0.035-0.267 for GO, demonstrating a favorable behavior toward picric acid adsorption.

The related Freundlich and Halsey isotherm parameters are calculated and tabulated in Table 3. The high correlation coefficients of Freundlich and Halsey models for the GO-Chi (0.9909) as compared to GO show that they are suitable for the interpretation of experimental data. On the other hand, the *n* value for GO-Chi was found 1.07. This indicates which the sorption of picric acid molecules is satisfactory at the described experimental conditions. Overall, these models could interpret the data reasonably well for the adsorption of picric acid on the GO-Chi. Hence, the assumption of multilayer adsorption by Freundlich and Halsey models is very well with the experimental data in the range of the studied concentrations for GO-Chi. In addition, the low correlation coefficients of Tempkin model for the GO (0.6728) and GO-Chi (0.8867) adsorbents show that this model is inappropriate for the picric acid adsorption on the both adsorbents.

3.4. Thermodynamics analysis

Table 3 shows the calculated thermodynamic parameters such as change in Gibbs free energy (ΔG˚), enthalpy (ΔH˚), and entropy (ΔS˚) for both adsorbents at three different temperatures. These parameters were estimated to investigate the spontaneity, feasibility and thermal properties of the adsorption process [56]. The ΔG˚ value could be obtained from the following equation with the previous calculation of the adsorption equilibrium constant (K_c):

$$\Delta G° = -RTln(K_c) \qquad (11)$$

$$K_c = \frac{C_s}{C_e} \qquad (12)$$

where C_s (mg/L), R and T are the concentration of picric acid on the adsorbent at equilibrium, the universal gas constant (8.314 J/mol K) and the temperature in kelvin, respectively. In addition, the change in ΔS˚ and ΔH˚ at a constant temperature (T) can be found from the Van't Hoff equation (equation13):

$$\ln K_c = (-\frac{\Delta H°}{R})\frac{1}{T} + \frac{\Delta S°}{R} \qquad (13)$$

The values of ΔS˚ and ΔH˚ were calculated from the intercept and slope, respectively of the linear plots of ln K_c versus *1/T*. The obtained values are given in Table 3. The results show

Table 3. The parameters of the different isotherm models and calculated thermodynamic for picric acid adsorption from aqueous solutions by GO and GO-Chi

Adsorbents	Isotherm models	The calculated parameters			
	Langmuir	**q_m(mg/g)**	**b(L/mg)**	**R^2**	**Plot**
GO	$\frac{C_e}{q_e} = \frac{1}{bq_m} + \frac{C_e}{q_m}$	2.59	0.275	0.9927	$\frac{C_e}{q_e}$ vs. C_e
GO-Chi		263.1	0.00338	0.2855	
	Freundlich	**K_f (mg/g)(mg/L)^n**	**n**	**R^2**	
GO	$\ln q_e = \ln K_f + \frac{1}{n} \ln C_e$	1.855	15.62	0.6866	ln q_e vs. ln C_e
GO-Chi		1.003	1.072	0.9909	
	Halsey	**K_H**	**n_H**	**R^2**	
GO	$\ln q_e = \frac{1}{n_H} \ln K_H - \frac{1}{n_H} \ln \frac{1}{C_e}$	1.6×10^4	15.62	0.6866	ln q_e vs. ln $\frac{1}{C_e}$
GO-Chi		1.003	1.072	0.9909	
	Tempkin	**K_1(L/g)**	**K_2**	**R^2**	
GO	$q_e = K_1 \ln K_2 + K_1 \ln C_e$	0.1478	2.1×10^5	0.6728	q_e vs. ln C_e
GO-Chi		13.968	0.228	0.8867	

The calculated thermodynamic parameters

	T (K)	K_c	ln K_c	ΔG°(kJ/mol)	ΔH°(kJ/mol)	ΔS°(kJ/mol K)
GO	298	0.266	-1.324	3.281	10.474	0.024
	313	0.332	-1.103	2.961		
	323	0.368	-1.000	2.601		
GO-Chi	298	2.600	0.956	-2.367	8.051	0.035
	313	2.670	0.982	-2.556		
	323	3.420	1.230	-3.302		

which the adsorption of picric acid onto GO is unspontaneous (positive values of ΔG°) and that is spontaneous for GO-Chi (negative values of ΔG°) under the conditions applied. In addition, decreasing ΔG° values with increasing temperature confirms the feasibility and spontaneity of the picric acid adsorption on the both adsorbents, in particular for GO-Chi. The positive values of ΔH° have indicated the endothermic nature of the picric acid adsorption on both adsorbents. In fact, the increase of temperature causes more efficient adsorption of picric acid on the adsorbents. It can be related to the easy desorption of water molecules from picric acid to bind on graphene surface [57]. The positive values of ΔS° demonstrated the increase in number of species at the solid-liquid interface and therefore an increased disorder was observed at the solid-solution interface during the adsorption process of picric acid onto the GO and GO-Chi. On the other hand, the ΔS° value of GO-Chi is more positive than that of

GO which it can be correspond to more accumulation and an increasing randomness of picric acid on the GO-Chi as compared to GO. In other words, the presence of a large number of adsorption positions on the GO-Chi result in the increase of picric acid adsorption and hence this topic follows the increase of entropy for GO-Chi in comparison with GO.

3.5. Desorption performance of GO-Chi

The synthesis route of GO-Chi after the treatment of GO with Chi is shown in Fig.6 along with the proposed mechanism of picric acid adsorption on the GO-Chi. According to Fig.6, there are three mechanisms for picric acid adsorption. First of all, the electrostatic interactions between OH (picric acid) and NH_2 (Chi) groups which results in the production of carboxylate ($-COO^-$) and ammonium ($-NH_3^+$) groups. The second mechanism is the interactions of hydrogen bond. Since picric acid has OH and NO_2 groups on its aromatic ring, these functional groups can form hydrogen bonds with NH_2 groups of Chi or the residual oxygen-containing groups of GO. In finally, the increased picric acid adsorption for the GO-Chi nanocomposite can be attributed to the contribution of GO through the π-π dispersion interaction between the aromatic ring of the picric acid and the GO planes. Because of the binding of carboxyl groups to chitosan, these interactions are expected to be stronger and cause more adsorption of picric acid.

Taking into account the practical application, the adsorption capacity and the desorption property are two key parameters to evaluate an adsorbent. An ideal adsorbent should not only possess higher adsorption capability, but also it show better desorption property, which will significantly reduce the overall cost for the adsorbents. Since the adsorption of picric acid onto GO-Chi composite is pH-dependent and a lower pH is beneficial, picric acid desorption from the adsorbent can be achieved by increasing the system pH values. The results showed which picric acid desorption increases with increasing pH values. As it was mentioned previously, an increase in the solution pH improves the solubility of picric acid which follows reduction of the interaction with the GO-Chi surface. On the other hand, the desorption behavior versus pH depends to the acid-base nature of picric acid. Thus, in pH>7, the negative charge density of picric acid increase which it lead to the higher electrostatic repulsion with GO-Chi surface. Therefore, the percentage of picric acid desorption from the GO-Chi at pH 9.0 was enhanced and its value about 80% was estimated. In addition, it can be found that adsorption percentage of the picric acid remains constant for 2 to 4 cycles of adsorption and desorption process and for fifth cycle of regeneration, adsorption percentage

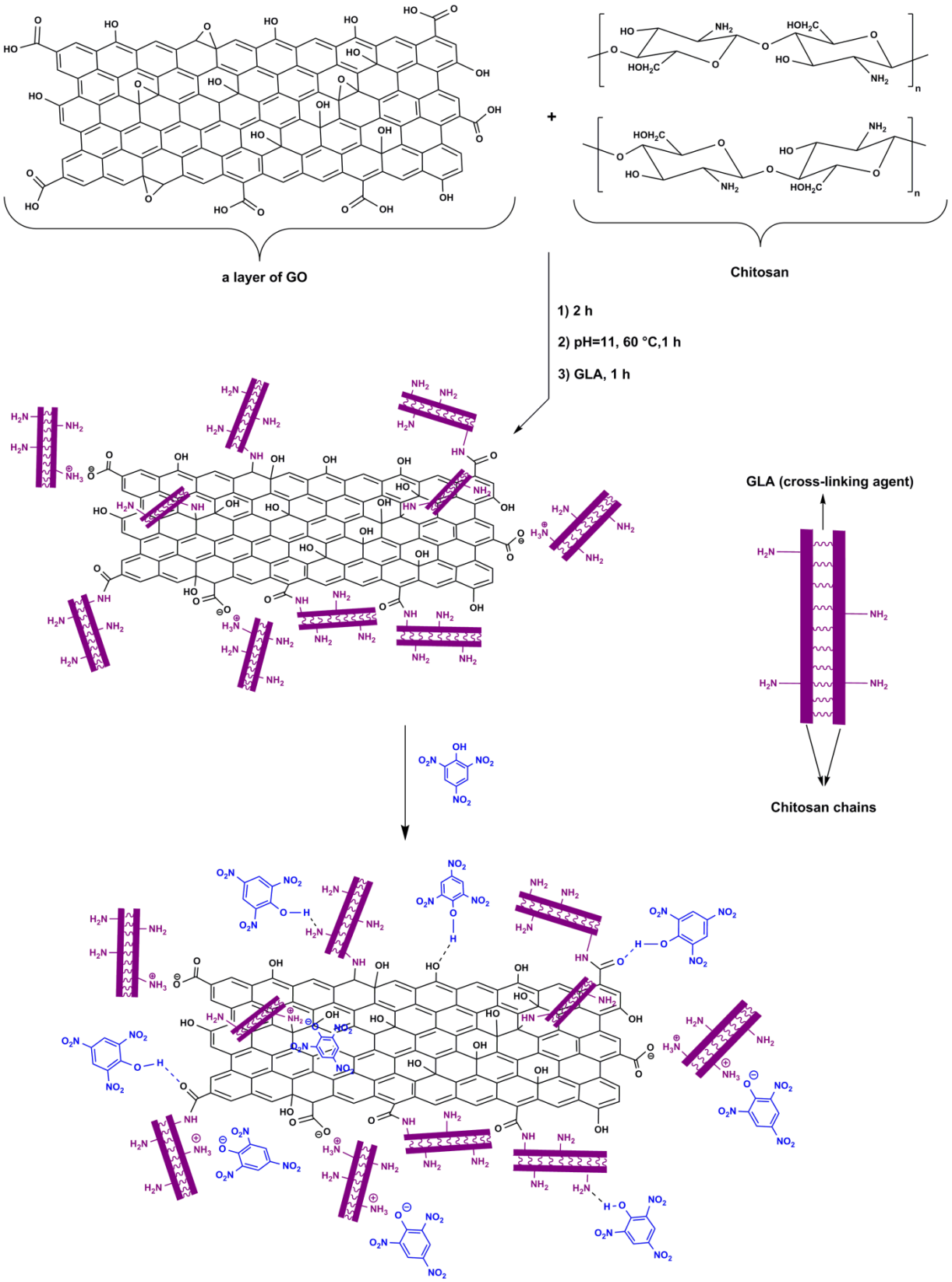

Fig. 6. The functionalization route of a GO layer by chitosan and the proposed mechanism for adsorption of picric acid onto the prepared GO-Chi.

decrease to 69.3% of the initial adsorption percentage. This reduction in the process can be related to the partial cleavage of the connection between the Chi and the GO sheets during regeneration process. This would mean that the hybrid can be reused as highly efficient recyclable sorption media but with less capacity than in the first cycle. The adsorption-desorption results indicates that the prepared GO-Chi nanocomposite could be an ideal picric acid adsorbent. The curves of the pH effect on the picric acid desorption and regeneration of GO-Chi is presented in Supplementary data.

4. Conclusion

We have firstly modified GO with Chi to form GO-Chi which was characterized by FT-IR, TGA, DTG, FESEM, EDX, XRD and BET. The study shows that GO-Chi has ideal performance for adsorption of picric acid. The results displayed that GO-Chi has higher sorption capacity respect to GO. The adsorption isotherms of picric acid have been well fitted by Freundlich and Halsey models for GO-Chi which mean physical adsorption happened. In addition, ΔG° values for GO-Chi were negative which show the practicability and spontaneity of the picric acid adsorption. The sorption kinetics was found to follow pseudo-second-order model for both adsorbents. Finally, the picric acid desorption from the GO-Chi was about 80% which this result is worthwhile since GO-Chi can be reused for 5 cycles of adsorption.

Acknowledgments

The financial and encouragement support provided by Research vice Presidency of Ayatollah Amoli branch, Islamic Azad University.

References

[1] M. Mende, D. Schwarz, C.Steinbach, R. Boldt, S. Schwarz, Simultaneous adsorption of heavy metal ions and anions from aqueous solutions on chitosan-Investigated by spectrophotometry and SEM-EDX analysis, Colloids and Surfaces A: Physicochemical and Engineering Aspects. 510 (2016) 275-282.

[2] G. Crini, P. Badot, Application of chitosan, a natural amino polysaccharide, for dye removal from aqueous solutions by adsorption processes using batch studies: A review of recent literature, Progress in Polymer Science. 33 (2008) 399-447.

[3] L. Zhang, Y. Zeng, Z. Cheng, Removal of heavy metal ions using chitosan and modified

chitosan: A review, Journal of Molecular Liquids. 214 (2016) 175-191.

[4] L. Zhang, H. Luo, P. Liu, W. Fang, J. Geng, A novel modified graphene oxide/chitosan composite used as an adsorbent for Cr(VI) in aqueous solutions, International Journal of Biological Macromolecules. 87 (2016) 586-596.

[5] S. Krishna Kumar, S.-J. Jiang, Chitosan-functionalized graphene oxide: A novel adsorbent an efficient adsorption of arsenic from aqueous solution, Journal of Environmental Chemical Engineering. 4 (2016) 1698-1713.

[6] H. Ge, Z. Ma, Microwave preparation of triethylenetetramine modified graphene oxide/chitosan composite for adsorption of Cr(VI), Carbohydrate Polymers. 131 (2015) 280-287.

[7] N. Van Hoa, T.T. Khong, T. Thi, H. Quyen, T. S. Trung, One-step facile synthesis of mesoporous graphene/Fe_3O_4/chitosan nanocomposite and its adsorption capacity for a textile dye, Journal of Water Process Engineering. 9 (2016) 170-178.

[8] S. Kumar, R.R. Nair, P.B. Pillai, S. Nath Gupta, M.A.R. Iyengar, Graphene Oxide-$MnFe_2O_4$ Magnetic Nanohybrids for Efficient Removal of Lead and Arsenic from Water, ACS Appl. Mater. Interfaces. 6 (2014) 17426-17436.

[9] N.A. Travlou, G.Z. Kyzas, N.K. Lazaridis, E.A. Deliyanni, Functionalization of Graphite Oxide with Magnetic Chitosan for the Preparation of a Nanocomposite Dye Adsorbent, Langmuir. 29 (2013) 1657-1668.

[10] N.E. Travlou, G.Z. Kyzas, N.K. Lazaridis, E.A. Deliyanni, Graphite oxide/chitosan composite for reactive dye removal, Chemical Engineering Journal. 217 (2013) 256-265.

[11] K. Gul, S.Sohni, M.Waqar, F.Ahmad, N.A.Nik Norulaini, M.Omar, Functionalization of magnetic chitosan with graphene oxide for removal of cationic and anionic dyes from aqueous solution, Carbohydrate Polymers. 152 (2016) 520-531.

[12] F. Wang, B.Yang, H. Wang, Q. Song, F. Tan, Y. Cao, Removal of ciprofloxacin from aqueous solution by a magnetic chitosan grafted graphene oxide composite, Journal of Molecular Liquids. 222 (2016) 188-194.

[13] P. Banerjee, S.R. Barman, A. Mukhopadhayay, P. Das, Ultrasound assisted mixed azo

dye adsorption by chitosan-graphene oxide nanocomposite, Chemical Engineering Research and Design. 117 (2017) 43-56.

[14] M.A. Kamal, S. Bibi, S. W.Bokhari, A. H.Siddique, T.Yasin, Synthesis and adsorptive characteristics of novel chitosan/graphene oxide nanocomposite for dye uptake, Reactive and Functional Polymers. 110 (2017) 21-29.

[15] M. Yusuf, F. M. Elfghi, S.A. Zaidi, E. C. Abdullahab, M. A. Khan, Applications of graphene and its derivatives as an adsorbent for heavy metal and dye removal: a systematic and comprehensive overview, RSC Adv. 5 (2015) 50392-50420.

[16] F. Yu, Y. Li, S. Han. J. Ma, Adsorptive removal of antibiotics from aqueous solution using carbon materials, Chemosphere. 153 (2016) 365-385.

[17] Z. Rappoport, The chemistry of phenols, John Wiley & Sons, 2003.

[18] J. Huang, X. Wang, Q. Jin, Y. Liu, Y. Wang, Removal of phenol from aqueous solution by adsorption onto OTMAC-modified attapulgite, Journal of Environmental Management. 84 (2007) 229-236.

[19] T.A. Lewis, D.A. Newcombe, L.R. Crawford, Bioremediation of soils contaminated with explosives. Journal of Environmental Management, 70 (2004) 291-307.

[20] M. Nipper, R.S. Carr, J.M. Biedenbach, R.L. Hooten, K. Miller, Fate and effects of picric acid and 2,6-DNT in marine environments: toxicity of degradation products, Marine Pollution Bulletin. 50 (2005) 1205-1217.

[21] R.J. Kavlock, L.A. Oglesby, L.L. Hall, H.L. Fisher, F. Copeland, T. Logsdon, M. Ebron-McCoy, In vivo and in vitro structure-dosimetry-activity relationships of substituted phenols in developmental toxicity assays, Fundament. Appl. Toxicol. 16 (1991) 225-229.

[22] P. Aggarwal, K. Misra, S.K. Kapoor, A.K. Bhalla, Effect of Surface Oxygen Complexes of Activated Carbon on the Adsorption of 2,4,6-Trinitrophenol, Defence Sci. J. 48 (1998) 219-222.

[23] USEPA, Technical Support Document for Water Quality Based Toxics Control, EPA/440/485032, United States Environmental Protection Agency, Washington DC, 1985.

[24] WHO (World Health Organization), Guidelines for Drinking Water Quality (vol. II): Health Criteria and Supporting Information, World Health Organization, Geneva, 1984.

[25] A. H. El-Sheikh, A.P. Newman, A.J. Said, A.M. Alzawahreh, M. M. Abu-Helal, Improving the adsorption efficiency of phenolic compounds into olive wood biosorbents by pre-washing with organic solvents: Equilibrium, kinetic and thermodynamic aspects, Journal of Environmental Management. 118 (2013) 1-10.

[26] Y. Park, G.A. Ayoko, E. Horváth, R. Kurdi, J. Kristof, R. L. Frost, Structural characterisation and environmental application of organoclays for the removal of phenolic compounds, Journal of Colloid and Interface Science. 393 (2013) 319-334.

[27] Z. Luo, M. Gao, S. Yang, Q. Yang, Adsorption of phenols on reduced-charge montmorillonites modified by bispyridinium dibromides: Mechanism, kinetics and thermodynamics studies, Colloids and Surfaces A: Physicochemical and Engineering Aspects. 482 (2015) 222-230.

[28] P.-T. Huong, B.-K. Lee, J. Kim, C.-H. Lee, Nitrophenols removal from aqueous medium using Fe-nano mesoporous zeolite, Materials & Design. 101 (2016) 210-217.

[29] T.-H. Pham, B.-K. Lee, J. Kim, Improved adsorption properties of a nano zeolite adsorbent toward toxic nitrophenols, Process Safety and Environmental Protection. 104 (2016) 314-322.

[30] P.Wang, L.Tang, X.Wei, G.Zeng, Y.Zhou, Y.Deng, J.Wang, Z.Xie, W.Fang, Synthesis and application of iron and zinc doped biochar for removal of p-nitrophenol in wastewater and assessment of the influence of co-existed Pb(II), Applied Surface Science. 392 (2017) 391-401.

[31] H. Tahermansouri, S. Gholitabar, Kinetic and multi-parameter isotherm studies of picricacid removal from aqueous solutions by carboxylated multi-walled carbon nanotubes in the presence and absence of ultrasound, Carbon Letters. 22 (2017) 14-24.

[32] B. Zhang, F. Li, T. Wu, D. Sun, Y. Li, Adsorption of p-nitrophenol from aqueous solutions using nanographite oxide, Colloids and Surfaces A: Physicochemical and Engineering Aspects. 464 (2015) 78-88.

[33] N.Z. Al-Mutairi, 2,4-Dinitrophenol adsorption by date seeds: Effect of physico-chemical environment and regeneration study, Desalination. 250 (2010) 892-901.

[34] A.M. Carvajal-Bernal, F. Gómez, L.Giraldo, J. C. Moreno-Piraján, Adsorption of phenol and 2,4-dinitrophenol on activated carbons with surface modifications, Microporous and Mesoporous Materials. 209 (2015) 150-156.

[35] H.Uslu, G. Ksel Demir, Adsorption of Picric Acid from Aqueous Solution by the Weakly Basic Adsorbent Amberlite IRA-67, J. Chem. Eng. Data. 55 (2010) 3290-3296.

[36] H.Sepehrian, J.Fasihi, M. Khayatzadeh Mahani, Adsorption Behavior Studies of Picric Acid on Mesoporous MCM-41, Ind. Eng. Chem. Res. 48 (2009) 6772-6775.

[37] D.Mohan, A.Sarswat, V.K. Singh, M. Alexandre-Franco, C.U. Pittman, Development of magnetic activated carbon from almond shells for trinitrophenol removal from water, Chemical Engineering Journal. 172 (2011) 1111-1125.

[38] S.K. Srivastava, V.K. Gupta, N.Johri, D.Mohan, Removal of 2,4,6-trinitrophenol using bagasse fly ash-A sugar industry waste material, Indian Journal of chemical technology. 2 (1995) 333-336.

[39] M. C. Hermosin, I. Pavlovic, M.A. Ulibarri, J. Cornejo, Hydrotalcite as sorbent for trinitrophenol: sorption capacity and mechanism, Water. Res. 30 (1996) 171-177.

[40] X.Zhang, C.Cheng, J.Zhao, L. Ma, S. Sun, C. Zhao, Polyethersulfone enwrapped graphene oxide porous particles for water treatment, Chem Eng. J. 215-216 (2013) 72-81.

[41] S. Lagergren, Zur theorie der sogenannten adsorption geloster stoffe, Kungliga Svenska Vetenskapsakademiens, Handlingar. 24 (1898) 1-39

[42] H. Tahermansouri, Z. Dehghan, F. Kiani, Phenol adsorption from aqueous solutions by functionalized multiwalled carbon nanotubes with a pyrazoline derivative in the presence of ultrasound, RSC Adv. 5 (2015) 44263-44273.

[43] H. Tahermansouri, R. Mohamadian Ahi, F. Kiani, Kinetic, equilibrium and isotherm studies of cadmium removal from aqueous solutions by oxidized multi-walled carbon nanotubes and the functionalized ones with thiosemicarbazide and their toxicity investigations: a comparison, J. Chin. Chem. Soc. 61 (2014) 1188-1198.

[44] S.H. Chien, W.R. Clayton, Application of Elovich equation to the kinetics of phosphate release and sorption in soils, Soil Sci. Soc. Am. J. 44 (1980) 265-268.

[45] W.J. Weber, J.C. Morris, Kinetics of adsorption on carbon from solution, J. Sanit. Eng. Div. 89 (1963) 31-59.

[46] I. Langmuir, The constitution and fundamental properties of solids and liquids, J. Am. Chem. Soc. 38 (1916) 2221-2295.

[47] H.M.F. Freundlich, Over the adsorption in solution, J. Phys. Chem. 57 (1906) 385-471.

[48] G.D. Halsey, The role of surface heterogeneity, Adv. Catal. 4 (1952) 259-269.

[49] M. Jahangiri, F. Kiani, H. Tahermansouri, A. Rajabalinezhad, The removal of lead ions from aqueous solutions by modified multi-walled carbon nanotubes with 1-isatin-3 thiosemicarbazone, Journal of Molecular Liquids. 212 (2015) 219-226.

[50] M. J. Tempkin, V. Pyzhev, Acta Physicochim.URSS.12 (1940) 327-356.

[51] H.H. Seung, Thermal reduction of graphene oxide, in: S. Mikhailov (Ed.), Physics and Applications of Graphene-Experiments, InTech, Rijeka, Croatia, 2011, pp.73-90.

[52] G. Z. Kyzas, N. A. Travlou, E. A. Deliyanni, The role of chitosan as nanofiller of graphite oxide for the removal of toxic mercury ions, Colloids and Surfaces B: Biointerfaces. 113 (2014) 467-476.

[53] S. Kumar, J. Koh, Physiochemical and optical properties of chitosan based grapheneoxide bionanocomposite, International Journal of Biological Macromolecules. 70 (2014) 559-564.

[54] K.S.W. Sing, D.H. Everett, R.A.W. Haul, L. Moscou, R.A.Pierotti, J. Rouquerol, T. Siemieniewska, Reporting physisorption data for gas/solid systems with special reference to the determination of surface area and porosity, Pure. Appl. Chem. 57 (1985) 603-619.

[55] A.P. Terzyk, Further insights into the role of carbon surface functionalities in the mechanism of phenol adsorption, J. Colloid Interface Sci. 268 (2003) 301-329.

[56] J.M. Smith, H.C. Van Ness (6th ed.), Introduction to Chemical Engineering Thermodynamics, McGraw-Hill, New York, 1987.

[57] T. Preočanin, F. Šupljika, N. Kallay, Charging of silver bromide aqueous interface: Evaluation of enthalpy and entropy of interfacial reactions from surface potential data, Journal of Colloid and Interface Science. 354 (2011) 318-321.